Yang-Mills correlation functions at finite temperature

Leonard Fister and Jan M. Pawlowski
Institut für Theoretische Physik, Universität Heidelberg, Philosophenweg 16, 69120 Heidelberg, Germany and ExtreMe Matter Institute EMMI, GSI Helmholtzzentrum für Schwerionenforschung mbH, Planckstr. 1, D-64291 Darmstadt, Germany

We put forward a continuum approach for computing finite temperature correlation functions in Yang-Mills theory. This is done in a functional renormalisation group setting which allows for the construction of purely thermal RG-flows. This approach is applied to the ghost and gluon propagators as well as the ghost-gluon vertex in the Landau gauge. We present results in a temperature regime going from vanishing temperature to temperatures far above the confinement-deconfinement temperature T_c. Our findings compare well with the lattice results available.

PACS numbers: 05.10.Cc, 11.15.Tk, 12.38.Aw, 11.10.Wx

I. INTRODUCTION

In the past two decades much progress has been made in our understanding of the QCD phase diagram. This has been achieved in a combination of first principle continuum computations in QCD, see e.g. [1–5], lattice simulations, see e.g. [6–8], as well as computations in low energy effective models for QCD, see e.g. [9–14]. All these methods have their specific strengths, and the respective investigations are complementary. In some applications, the methods have even been applied in combination.

In recent years the first principle continuum approach as well as the model computations have become far more quantitative. This is the more interesting as at present they are one of the methods of choice for finite density and non-equilibrium investigations that are necessary for an understanding of heavy ion collisions. A full quantitative understanding of the phase diagram of QCD from these methods requires a good quantitative grip on the thermodynamics and finite temperature dependence of Yang-Mills theory, for a review on thermal gluons see [15], for applications of Dyson-Schwinger equations (DSEs) for Yang-Mills propagators see e.g. [16, 17].
However, quantitatively reliable continuum results for correlation functions in Yang-Mills theory at general temperatures are presently not available. This concerns in particular the transition region of the confinement-deconfinement phase transition, occurring at the critical temperature T_c. The same applies to thermodynamic quantities such as the pressure. Computations in Yang-Mills theory done with hard-thermal loop or 2PI resummations do not match the lattice results for temperatures $T \lesssim 3\,T_c$, see e.g. [18] and references therein. In turn, they are reliable for $T \gg T_c$.

In the present work we put forward an approach with the functional renormalisation group (FRG), for QCD-related reviews see [1, 19–25]. The FRG incorporates non-perturbative effects by a successive integration of fluctuations related to a given momentum scale, also at non-vanishing temperature, for applications in Yang-Mills theory see e.g. [19, 26–29]. It is applicable to all temperatures, in particular also for temperatures $T \lesssim 3\,T_c$. The present implementation of the FRG incorporates only thermal fluctuations, see e.g. [29], and utilises the vacuum physics at vanishing temperature as an input. This also allows us to study the effect of global gauge fixing issues in the Landau gauge due to the Gribov problem, for detailed discussions see [30, 31]. A summary of the present work and results is also presented in [32].

In Section II we give a brief introduction to the FRG-approach to Yang-Mills theory. In particular, it is illustrated at the example of the two-point correlation functions, how flow equations for correlation functions are derived from the flow of the effective action.

Section III is devoted to the important issue of locality of an FRG-flow. We show how to minimise the momentum transfer present in the diagram, and hence to minimise the sensitivity to the approximation at hand. We also discuss the factorisation of diagrams at large external momenta that is relevant for subleading momentum corrections.

In Section IV we introduce the flow for thermal fluctuations as that of the difference of flows at finite temperature and vanishing temperature, see [29]. The locality introduced in Section III is used for improving the stability of this difference, as well as having access to a trivial initial condition for the thermal flow at large cutoff scales. Variants of which have been very successfully used already for the physics of scalar theories as well as fermion-boson mixtures, for reviews see [24, 33, 34].

The approximation used in the present work is detailed in Section V, and some computational details are discussed in Section VI. Results for propagators and vertices are presented in the Sections VII. They are compared to lattice results, [15, 17, 35–44]. Our observations are shortly summarised in Section VIII.

II. YANG-MILLS CORRELATION FUNCTIONS FROM RG-FLOWS

In this section we introduce the functional RG setting for Yang-Mills theories which we use for the computation

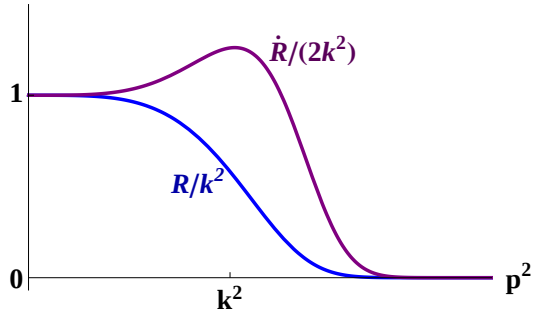

FIG. 1: Regulator $R(p^2)$ and its (logarithmic) cut-off scale derivative $\partial_t R(p^2) = \dot{R}(p^2)$.

of propagators and vertices. Central to this approach is the scale-dependent effective action Γ_k, where quantum fluctuations with momenta $p^2 \gtrsim k^2$ are already integrated out, and k denotes an infrared cut-off scale. By varying the cut-off scale k one thereby interpolates between the classical action in the ultraviolet and the full quantum effective action in the infrared, where the cut-off is removed. An infinitesimal change of k is described by a flow equation for Γ_k, and the interpolation can be achieved by integrating this flow.

Within the standard Faddeev-Popov gauge fixing procedure in the Landau gauge,

$$\partial_\mu A^a_\mu = 0\,, \qquad a = 1, ..., N_c^2 - 1, \tag{1}$$

the classical gauge fixed action for $SU(N_c)$ Yang-Mills theory in Euclidean space-time is given by

$$S = \int_x \left(\frac{1}{4} F^a_{\mu\nu} F^a_{\mu\nu} + \bar{c}^a \partial_\mu D^{ab}_\mu c^b \right) , \tag{2}$$

with $\int_x = \int d^4x$. In (2) we have already introduced the ghost action with the ghost fields $\bar{c}^a$ and c^a. The field strength F and the covariant derivative D are given by

$$\begin{aligned} F^a_{\mu\nu} &= \partial_\mu A^a_\nu - \partial_\nu A^a_\mu + g f^{abc} A^b_\mu A^c_\nu \,, \\ D^{ab}_\mu &= \delta^{ab} \partial_\mu + g f^{acb} A^c_\mu \,. \end{aligned} \tag{3}$$

The gauge fields are transveral due to the Landau gauge (1). Hence operators and the inverse of operators are defined on the transversal subspace. The suppression of the infrared fluctuations is achieved via a modification of the propagator with $S \to S + \Delta S_k$ and

$$\Delta S_k = \frac{1}{2} \int_p A^a_\mu \, R^{ab}_{\mu\nu} \, A^b_\nu + \int_p \bar{c}^a \, R^{ab} \, c^b \,, \tag{4}$$

with $\int_p = \int d^4p/(2\pi)^4$. The momentum-dependent regulator functions $R^{ab}_{\mu\nu}$ and R^{ab} implement the infrared cut-off at the momentum scale $p^2 \approx k^2$ for gluon and ghost respectively. They carry a Lorentz and gauge group tensor structure and are proportional to a dimensionless shape function r, schematically we have $R(p^2) \propto p^2 \, r(p^2/k^2)$.

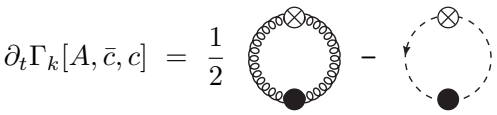

FIG. 2: Functional flow for the effective action. Lines with filled circles denote fully dressed field dependent propagators (7). Crossed circles denote the regulator insertion $\partial_t R_k$.

An example for $R(p^2)$ and its logarithmic scale derivative is given in Fig. 1. As we work in Landau gauge, (1), we can restrict ourselves to a transversal gluon regulator, $p_\mu R^{ab}_{\mu\nu}(p) = 0$.

With the notation $\varphi = (A, c, \bar{c})$ we write the flow equation for the Yang-Mills effective action $\Gamma_k[A, c, \bar{c}]$ at finite temperature T as

$$\begin{aligned} \partial_t \Gamma_k[\varphi] \;=\; & \frac{1}{2} \sum\!\!\!\!\!\!\int_p \, G^{ab}_{\mu\nu}[\varphi](p,p) \, \partial_t R^{ba}_{\nu\mu}(p) \\ & - \sum\!\!\!\!\!\!\int_p \, G^{ab}[\varphi](p,p) \, \partial_t R^{ba}(p) \,, \end{aligned} \tag{5}$$

where $t = \ln k$, and the momentum integration measure at finite temperature is given by

$$\sum\!\!\!\!\!\!\int_p = T \sum_{n \in \mathbb{Z}} \int \frac{d^3p}{(2\pi)^3} \,, \quad \text{with} \quad p_0 = 2\pi T n \,, \tag{6}$$

where the integration over p_0 turns into a sum over Matsubara frequencies. Both, gluons and ghosts have periodic boundary conditions, $\varphi(x_0 + 1/T, \vec{x}) = \varphi(x_0, \vec{x})$, which is reflected in the Matsubara modes $2\pi T n$ with a thermal zero mode for $n = 0$. At vanishing temperature we have $\sum\!\!\!\!\!\!\int \to \int_p$. The full field dependent propagator for a propagation from φ_1 to φ_2 is given by

$$G_{\varphi_1\varphi_2}[\varphi](p,q) = \left(\frac{1}{\Gamma^{(2)}_{T,k}[\varphi] + R_k} \right)_{\varphi_1\varphi_2} (p,q) \,. \tag{7}$$

In (7) we also used the regulator function in field space, $R_{k,\varphi_1\varphi_2}$ with

$$R_{k,A^a_\mu A^b_\nu} = R^{ab}_{\mu\nu} \,, \qquad R_{k,\bar{c}^a c^b} = -R_{k,c^b \bar{c}^a} = R^{ab} \,. \tag{8}$$

The flow is finite in both, the infrared and the ultraviolet, by construction. Effectively, the momentum integration in (5) only receives contributions for momenta in the vicinity of $p^2 \lesssim k^2$. Consequently, it has a remarkable numerical stability. The flow solely depends on dressed vertices and propagators, leading to consistent RG-scaling on either side of (5). Diagrammatically, the flow in (5) is depicted in Fig. 2.

The structure of the flow (5), or Fig. 2, is more appar-

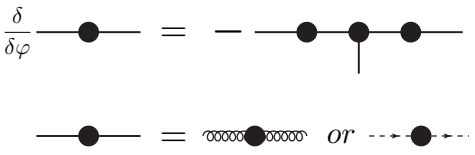

FIG. 3: Field derivative of the propagator. The solid line stands for either a gluon or a ghost propagator and the vertex is depicted by a filled circle.

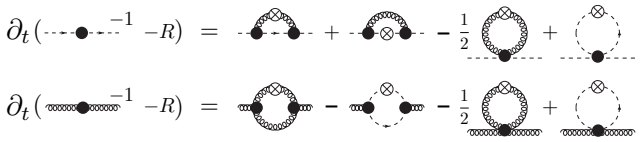

FIG. 4: Flow equations for the ghost and gluon propagators. Vertices with filled circles denote fully dressed vertices. All propagators are fully dressed, the filled circles for the internal ones have been omitted for the sake of clarity. Crossed circles denote the regulator insertion $\partial_t R_k$.

ent in a formulation with the fields φ. Written in these fields the cut-off term reads $\Delta S_k[\varphi] = \frac{1}{2}\varphi \cdot R_k \cdot \varphi$, where the dot indicates the contraction over species of fields including space-time or momenta, Lorentz and gauge group indices. Note that the cut-off term now includes two times the ghost term which cancels the global factor 1/2 and leads to (4). In this short hand notation the flow equation takes the simple and concise form

$$\partial_t \Gamma_k[\varphi] \;=\; \frac{1}{2}\mathrm{Tr}\, G[\varphi](p,p)\cdot \partial_t R_k(p)\,, \tag{9}$$

where the trace includes a relative minus sign for the ghosts. Eq. (9) is well-suited for structural considerations.

Flow equations for propagators and vertices are obtained from (5) or (9) by taking derivatives with respect to φ. The computation of φ-derivatives on the rhs of (9) only requires the equation for the field derivative of the propagator and the notion of the full one-particle irreducible (1PI) n-point functions. The latter are defined by

$$\Gamma_k^{(n)}(p_1,...,p_n) = \frac{\delta \Gamma_k}{\delta\varphi(p_1)\cdots\varphi(p_n)}\,. \tag{10}$$

The field derivative of the propagator is given by

$$\frac{\delta}{\delta\varphi} G[\varphi] = -G[\varphi]\cdot\Gamma_k^{(3)}[\varphi]\cdot G[\varphi]\,, \tag{11}$$

and diagrammatically depicted in Fig. 3. With the above equations one readily derives the flow of 1PI n-point functions. Again, this can be nicely illustrated diagrammatically at the example of the propagators, which are the key objects in the approach. We take two field derivatives of the flow equation. Applying this to its diagrammatical form displayed in Fig. 2 we are led to the flow equations given in Fig. 4. The flow equations only contain one loop diagrams in the full propagators, which is a consequence of the exact one-loop form of the flow for the effective action, see (5) and Fig. 2. Moreover, they only depend on the full vertices (10). Analogously to the flow of the two-point functions, the flows of n-point functions only contain one-loop diagrams that depend on full propagators and vertices.

The propagators and vertices are purely transversal due to the transversality of the gauge field. The purely transversal correlation functions vanish by contracting one of the Lorentz indices with its momentum, $(p_i)_{\mu_i}\Gamma^{(n)\,T}_{\mu_1\cdots\mu_i\cdots\mu_m} = 0$ for $i = 1,...,m$. Note that in general $n \neq m$ due to the ghosts. Since the propagators are purely transversal in the Landau gauge, the purely transversal correlation functions in the Landau gauge form a closed system of flow equations: the flow of a purely transversal correlation function only depends on purely transversal correlation functions and carry the whole dynamics. Any observables can be built-up from the purely transversal correlation functions.

In turn, the flow of correlation functions with at least one longitudinal direction, $\Gamma^{(n)\,L}$, depends on both, $\Gamma^{(n)\,T}$ and $\Gamma^{(n)\,L}$. Moreover, they also obey modified Slavnov-Taylor identities, see [21, 22, 45, 46] and references therein.This situation is summarised in

$$\begin{aligned}
\partial_t \Gamma^{(n)\,T} &= \mathrm{Flow}_n^T[\{\Gamma^{(m)\,T}\}]\,,\\
\partial_t \Gamma^{(n)\,L} &= \mathrm{Flow}_n^L[\{\Gamma^{(m)\,T},\Gamma^{(m)\,L}\}]\,,\\
(p)_\mu \Gamma^{(n)\,L}_{\mu\mu_2\cdots\mu_m} &= \mathrm{mSTI}_n[\{\Gamma^{(m)\,T},\Gamma^{(m)\,L}\}]\,,
\end{aligned} \tag{12}$$

where $m \leq n+2$. The modified Slavnov-Taylor identities converge to the standard ones for vanishing cut-off scale $k = 0$. The above system comprises the full information about the correlation functions in the Landau gauge. Interestingly, the hierarchy of flow equations for the purely transversal correlation functions can be solved independently and carries the full dynamics of Yang-Mills theory. In this context we remark that vertex constructions aided by Slavnov-Taylor identities implicitly utilise an assumed uniformity of correlation functions, that is

$$\partial_{p_\mu}\Gamma^{(n)} < \infty \quad \text{for all } (p_1,...,p_n)\,. \tag{13}$$

This works well in perturbation theory but has to be taken with a grain of salt in the non-perturbative regime.

It is also worth emphasising that (12) does not depend on the way how the Landau gauge is introduced. The Landau gauge can be also represented as the limit of covariant gauges with the gauge action $1/(2\xi)\int_x(\partial_\mu A^a_\mu)^2$ and gauge fixing parameter ξ. Here $\xi = 0$ signals the Landau gauge. In this case in general one also introduces a regularisation for the gauge mode, schematically given

by

$$R^{\rm L} = \lim_{\xi\to 0}\frac{1}{\xi}\Pi^L\, p^2 r(p^2/k^2)\,, \tag{14}$$

with the projection operators

$$\begin{aligned}\Pi^T_{\mu\nu}(p) &= \delta_{\mu\nu} - p_\mu p_\nu/p^2\,,\\ \Pi^L_{\mu\nu}(p) &= p_\mu p_\nu/p^2\,.\end{aligned} \tag{15}$$

on transversal and longitudinal degrees of freedom, respectively. Still, the longitudinal mode does not play any rôle for the flow of correlation functions as $G\cdot\partial_t R^{\rm gauge}\cdot G\to 0$ for $\xi\to 0$ and $\lim_{\xi\to 0} G$ is purely transversal. Note however, that $1/2\,{\rm Tr}\,R^{\rm gauge}\cdot G$ does not vanish. Upon t-integration it gives the thermal pressure for the gauge mode, namely the Stefan-Boltzmann pressure of N_c^2-1 fields, see [29].

III. LOCALITY OF RG-FLOWS

The loops on the rhs of Fig. 4 only received contributions from momentum fluctuations with $p^2\lesssim k^2$ due to the regulator insertion $\partial_t R$, see Fig. 1. However, the external momenta are not limited by such a constraint. Indeed, for large external momenta, $p^2/k^2\gg 1$ the flow factorises at leading order: the tadpole diagram with the four-gluon vertex tends to a constant. The other tadpole diagrams vanish with powers $\lesssim k^2/p^2$. The related four-point functions are not present on the classical level and hence decay at least with k^2/p^2. This intuitive statement can be proven easily with the help of the respective flows and the factorisation present there. Here, we explain the factorisation at the relevant example of the three-point function diagrams, see also Fig. 5 for the example of the flow of the ghost propagator. These diagrams factorise for large external momenta, one factor being the uncutted internal line evaluated at p^2. For $p^2/k^2\to\infty$ we have,

$$\begin{aligned}&{\rm Tr}\,\left[\left(G\dot{R}G\right)(q)\cdot\Gamma^{(3)}(q,p+q)\cdot G(p+q)\cdot\Gamma^{(3)}(q+p,q)\right]\\ &\to\ {\rm Tr}\,\left[\left(G\dot{R}G\right)(q)\cdot\Gamma^{(3)}(0,p)\cdot G(p)\cdot\Gamma^{(3)}(p,0)\right]\\ &\quad +\,\text{higher order terms}\,,\end{aligned} \tag{16}$$

where the trace also integrates over loop momenta q. In (16) we have assumed that all momentum components are suppressed by the regulator: R is a function of p^2 and not e.g. of solely spatial momentum squared, $\vec{p}^2$. Note also that for kinetic and/or symmetry reasons the leading order in line two of (16) may vanish. This even supports the factorisation. The interchange of integration and limit and hence the factorisation works as the diagram is still finite with the uncutted line being removed.

The general factorisation in (16) can be nicely illustrated diagrammatically at the example of the flow of the ghost propagator Fig. 4. In Fig. 5 we display the factorisation of the first diagram in Fig. 4. The terms in the second line of (16) or on the rhs of Fig. 5 are already subleading as the flow usually is peaked at momentum scales $p^2\lesssim k^2$. However, they are already quantitatively relevant at vanishing temperature but turn out to be crucial for the correct thermodynamics, in particular for the slow approach to the Stefan-Boltzmann limit for large temperatures. Potentially, they also play an important rôle for the thermodynamics in non-relativistic systems, where they supposedly relate to the Tan-relations [47–49] in the context of many-body physics; for FRG-reviews see e.g. [33, 34].

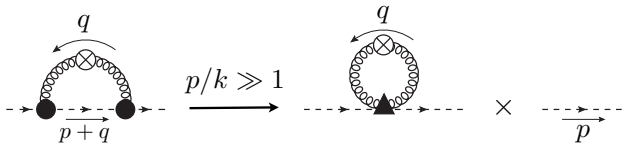

FIG. 5: Factorisation in leading order for large momenta for the first diagram (cutted gluon line) in the flow of the (inverse) ghost propagator in Fig. 4 . The triangle stands for the product of the two vertices at $q=0$ and reads $-p_\mu p_{\mu'} f^{acd} f^{bc'd'}$.

Still we have to reconcile the above polynomial decay with external momenta p with the well-known exponential decay of thermal fluctuations with the standard suppression factor $\exp(-m/T)$ in the presence of a mass scale m. In the present case, this mass scale can be either the cut-off scale k or the physical mass scale of Yang-Mills theory, $\Lambda_{\rm QCD}$, which is directly linked to the critical temperature T_c of the confinement-deconfinement phase transition. The exponential thermal damping factor originates from the full Matsubara sum, and is strictly not present if only the lowest Matsubara frequencies are taken into account. A four-dimensional regulator depending on four-dimensional loop momentum $q^2=(2\pi T n)^2+\vec{q}^2$ cuts the Matsubara sum, and hence only leads to the polynomial decay of the flow. The exponential suppression is then built-up successively with the flow. The above properties can be already very clearly seen and understood at the example of perturbative one-loop flows.

The full Matsubara sum is reintroduced for regulators only depending on $\vec{p}^2$. They are frequently used in finite temperature applications of the FRG as they allow for an analytic summation of the Matsubara sums if only the trivial frequency dependence is taken into account, see e.g. [19, 29, 50, 51]. However, in the present work we consider full propagators and vertices, that is with non-trivial frequency and momentum dependence. Moreover, as lower-dimensional regulators introduce an additional momentum or frequency transfers in the flow we therefore refrain from using them here.

Apparently, the large momentum contributions also weaken the locality of the flow present in the loop momenta as they induce a momentum transfer: the flows at

a given cut-off scale k carry physics information about larger momentum scales. In turn this entails that any local approximation does not fully cover this momentum transfer. Now we utilise the freedom of reparameterising the effective action as well as the choice of the regulator in order to reinstall the locality of the flow for the two-point functions $\Gamma_k^{(2)}$. This minimises the systematic error of a given approximation, see [21]. To that end, we rewrite the regulator term in (4) as follows,

$$\Delta S_k = \frac{1}{2}\int_p A^\mu_{k,a}\,\hat R^{ab}_{\mu\nu}\,A^\nu_{k,b} + \int_p \bar c_{k,a}\,\hat R^{ab}\,c_{k,b}\,. \qquad (17)$$

The fields $\phi = (A_k, c_k, \bar c_k)$ in (17) relate to the cut-off independent fields $\varphi = (A, c, \bar c)$ in the classical action via a cut-off and momentum dependent rescaling,

$$\phi(p) = \hat Z^{1/2}_{\phi,k}(p)\varphi(p) \quad \text{with} \quad \partial_t\phi(p) = \hat\gamma_\phi(p)\,\phi(p)\,, \qquad (18)$$

where the derivative is taken at fixed φ. We will use the natural definition $\hat\gamma_{\bar c} = \hat\gamma_c$. Eq. (18) implies

$$\hat\gamma_\phi(p) = \partial_t \log \hat Z_\phi(p)\,, \quad \text{and} \quad R = \hat Z\cdot\hat R\,. \qquad (19)$$

The field reparametrisation in (18) does not change the effective action, in particular the regulator term ΔS_k does not change. It simply amounts to rewriting the effective action in terms of the new fields,

$$\hat\Gamma_k[\phi] = \Gamma_k[\varphi]\,. \qquad (20)$$

Then, ϕ-derivatives $\hat\Gamma_k^{(n)}$ of the effective action $\Gamma_k = \hat\Gamma_k$ are given by (10) with $\varphi \to \phi$,

$$\hat\Gamma_k^{(n)}(p_1,...,p_n) = \frac{\delta\hat\Gamma_k}{\delta\phi(p_1)\cdots\delta\phi(p_n)}\,. \qquad (21)$$

As the fields ϕ and φ only differ by a momentum dependent rescaling with $\hat Z^{1/2}$, the correlation functions are related by a simple rescaling with powers of $\hat Z^{1/2}$,

$$\Gamma^{(n)}(p_1,...,p_n) \;=\; \prod_{i=1}^n \hat Z^{1/2}_{\phi_i}(p_i)\,\hat\Gamma^{(n)}(p_1,...,p_n)\,. \qquad (22)$$

The rescaling with $\hat Z$ is up to our disposal, and we shall use it to minimise the momentum transfer in the flow equation of the two-point function by eliminating the subleading terms in the flow exemplified in (16). Note that this does not remove the related contributions, the momentum transfer is still present but does not feedback directly in the flow, see [21]. This is also elucidated below.

The flow equation for the effective action now receives further contributions from the k-dependence of the fields ϕ. We are finally led to the following flow for $\hat\Gamma_{k,T}[\phi] = \Gamma_k[\varphi]$, see [21],

$$\begin{aligned}\left(\partial_t + \sum_i \sum\!\!\!\!\!\!\int_p \hat\gamma_{\phi_i}(p)\phi_i(p)\frac{\delta}{\delta\phi_i(p)}\right)\hat\Gamma_{T,k}[\phi] = \\ \frac{1}{2}\sum\!\!\!\!\!\!\int_p \hat G^{ab}_{\mu\nu}[\phi](p,p)\,(\partial_t + 2\hat\gamma_A(p))\hat R^{ba}_{\nu\mu}(p) \\ -\sum\!\!\!\!\!\!\int_p \hat G^{ab}[\phi](p,p)\,(\partial_t + 2\hat\gamma_C(p))\hat R^{ba}(p)\,, \qquad (23)\end{aligned}$$

where $\hat G[\phi](p,q) = \big(\hat\Gamma_k^{(2)}[\phi] + \hat R\big)^{-1}(p,q)$ denotes the full regularised propagator for the propagation of ϕ, see (7) with $\varphi \to \phi$ and $\Gamma_k^{(2)} \to \hat\Gamma_k^{(2)}$. The functional flow in (23) looks rather complicated, but it is simply a reparameterisation of the standard flow in (5), or (9). In the condensed notation introduced in Section II this is more apparent, the flow equation (23) then reads

$$\left(\partial_t + \phi\cdot\hat\gamma_\phi\cdot\frac{\delta}{\delta\phi}\right)\hat\Gamma_{T,k}[\phi] = \frac{1}{2}\mathrm{Tr}\,\hat G[\phi]\cdot\,(\partial_t + 2\hat\gamma_\phi)\cdot\hat R_k\,. \qquad (24)$$

Eq. (24) illustrates that we have only reparametrised the fields in a scale-dependent way.

Taking two derivatives with respect to $\phi_1(p)$ and $\phi_2(q)$ of (23) at vanishing ghost fields and constant gauge field we schematically get the flow

$$(\partial_t + \hat\eta_{\phi_1}(p)\,)\,\hat\Gamma^{(2)}_{\phi_1\phi_2}(p) = \mathrm{Flow}^{(2)}_{\phi_1\phi_2}(p)\,, \qquad (25)$$

where the rhs of (25) stands for the $\phi_1(p)$ and $\phi_2(q)$ derivative of the rhs of (23),

$$\mathrm{Flow}^{(2)}_{\phi_1\phi_2} = \frac{\delta^2}{\delta\phi_1\delta\phi_2}\left(\frac{1}{2}\mathrm{Tr}\,\hat G[\phi]\cdot\,(\partial_t + \hat\eta_\phi)\cdot\hat R_k\right)\,, \qquad (26)$$

and

$$\hat\eta_\phi(p) = 2\hat\gamma_\phi(p) = \partial_t\log\hat Z_k(p)\,, \qquad (27)$$

is the 'anomalous' dimension of the propagator related to the rescaling of the fields with $\hat Z$. In (25) we have used that for vanishing ghosts the two-point functions are diagonal/symplectic in field space. The only non-vanishing components are $\hat\Gamma^{(2)}_{k,AA}$ and $\hat\Gamma^{(2)}_{k,c\bar c} = -\hat\Gamma^{(2)}_{k,\bar c c}$. The two-point functions for constant gauge fields are also diagonal in momentum space, that is

$$\begin{aligned}\hat\Gamma^{(2)}_k(p,q) \;&=\; \hat\Gamma^{(2)}_k(p)(2\pi)^4\delta(p-q)\,, \\ \mathrm{Flow}^{(2)}(p,q) \;&=\; \mathrm{Flow}^{(2)}(p)(2\pi)^4\delta(p-q)\,, \qquad (28)\end{aligned}$$

and the relation (22) for the two-point functions reads

$$\Gamma^{(2)}(p) = \hat Z(p)\,\hat\Gamma^{(2)}(p)\,. \qquad (29)$$

Now we can come back to the question of locality of the flow. Our aim is to remove the large momentum tail displayed in (16) from the flow in order to keep its locality

in momentum space, i.e. to minimise the momentum transfer. This is achieved by demanding

$$\partial_t \hat{\Gamma}_k^{(2)}(p)\Big|_{p^2>(\lambda k)^2} \equiv 0\,, \tag{30}$$

which implies

$$\hat{\eta}_\phi(p) \;=\; \frac{\mathrm{Flow}^{(2)}(p)}{\hat{\Gamma}_k^{(2)}(p)}\theta(p^2-(\lambda k)^2)\,. \tag{31}$$

Eq. (30) entails that the momentum transfer is switched off for momenta larger than the cut-off scale. The factor λ controls this scale and can be used for an error estimate.

After having computed the localised correlation functions $\hat{\Gamma}^{(n)}$, we can derive the correlation functions $\Gamma^{(n)}$ via rescaling with powers of $\hat{Z}$, see (21),(29). The scaling factor is computed by integrating $\hat{\eta}_k$ defined in (27),

$$\hat{Z}_k(p;T) \;=\; \hat{Z}_{k=0}(p;T)\,\exp\left\{\int_0^k dt'\;\hat{\eta}_{k'}(p;T)\right\}\,. \tag{32}$$

This determines $\hat{Z}_k$ up to a k-independent function, and we use

$$\hat{Z}_{\phi,k=0}(p;T=0)=1\,. \tag{33}$$

For the choice (33) the two sets of correlation functions agree in the vacuum at $k=0$.

As the flow of general correlation functions can be written down solely in terms of $\hat{\Gamma}^{(n)}$, the relation (30) with (31) eliminates the momentum transfer (in $\Gamma^{(2)}$) from the flow. Note however, that a remnant of it is still present via the factor $2\hat{\gamma}_\phi=\hat{\eta}_\phi$ on the rhs of the flow (24). For regulators that decay sufficiently fast for momenta $p^2\gg k^2$ this is quantitatively negligible. Indeed, for regulators which vanish identically for momenta bigger than λk the momentum transfer now is described solely by $\hat{\eta}_\phi(p)$ and decouples completely. We also remark in this context, that the above construction and the definition (33) leading to (30) with $\lambda=1$ can be deduced by evoking functional optimisation for momentum-dependent approximations, see [21]. The above heuristic arguments entail that optimisation restores the locality of the flow also in general momentum- and frequency-dependent approximations.

IV. THERMAL FLUCTUATIONS

The flow equation (5) includes both, quantum as well as thermal fluctuations. For the present purpose we are interested in the thermal fluctuations, for reviews on thermal FRG see e.g. [19, 52, 53]. Thermal fluctuations are encoded in the difference of the flows at finite and at vanishing temperature, see e.g. [29],

$$\partial_t\Delta\Gamma_{T,k}[\phi] = \frac{1}{2}\mathrm{Tr}\,G[\phi]\cdot\partial_t R\Big|_T - \frac{1}{2}\mathrm{Tr}\,G[\phi]\cdot\partial_t R\Big|_{T=0}\,, \tag{34}$$

where

$$\Delta\Gamma_{T,k}[\phi]=\Gamma_k[\phi]|_T-\Gamma_k[\phi]|_{T=0} \tag{35}$$

accounts for the difference between the effective action at vanishing and at finite temperature. Due to the thermal exponential suppression the flow (34) should have locality properties with respect to the scale $k=T$. As discussed in the previous section, locality is important for the quantitative reliability of a given approximation. In the present work we implement this idea as follows: We use the vacuum physics at vanishing temperature as input for the flow. A given set of correlation functions $\Gamma^{(n)}_{k=0}$ at $T=0$ and $k=0$ can be integrated with the flow (5) at vanishing temperature in a given approximation up to a large momentum scale $k=\Lambda$,

$$\Gamma^{(n)}_{k=0}(p_1,...,p_n)\Big|_{T=0} \stackrel{\text{flow}}{\longrightarrow} \Gamma^{(n)}_{k=\Lambda}(p_1,...,p_n)\Big|_{T=0}\,. \tag{36}$$

In the approximation at hand, (36) defines the initial conditions $\Gamma^{(n)}_{k=\Lambda}\Big|_{T=0}$, which give the correct vacuum correlation functions if integrated to $k=0$. The ultraviolet scale Λ is chosen such that all thermal fluctuations are suppressed given the maximal temperature to be considered, $T_{\max}$. This implies

$$\frac{T_{\max}}{\Lambda}\ll 1\,. \tag{37}$$

Then, switching on $T\leq T_{\max}$ does not change the initial conditions at leading order, i.e.

$$\frac{1}{\Lambda^{d_n}}\Delta\Gamma^{(n)}_{T,\Lambda}(p_1,...,p_n)=0+O\left(\frac{T}{\Lambda}\right)\,, \tag{38}$$

where d_n is the canonical dimension of $\Gamma^{(n)}$, and all momenta are of order Λ or bigger, $p_i^2\gtrsim\Lambda^2$, see e.g. [54] for scalar theories. This suggests that we can flow $\Delta\Gamma_{T,k}$ from the trivial initial condition (38) to vanishing cut-off $k=0$. Note also that within such an approach to thermal fluctuations, it is only the difference $\partial_t\Delta\Gamma_{T,k}$ which is sensitive to the approximation at hand. We illustrate the procedure outlined above in a heuristic plot, see Fig. 6.

In this context it is also worth discussing the rapidity of $\Delta\Gamma^{(n)}_{T,\Lambda}\to 0$ for large cut-off scales $k=\Lambda$. This is linked to the question of locality raised in the previous Section III. In Fig. 6 it is indicated that $\Delta\Gamma^{(n)}_{T,k}$ start to significantly deviate from zero at the thermal scale $k\approx 2\pi T$. Above and in the previous section we have argued that we only have a polynomial suppression for the flow $\Delta\dot{\Gamma}^{(n)}_{T,k}$. Note also, that the longer $\Delta\Gamma^{(n)}_{T,k}$ survives at large scales $k\to\Lambda$ the more sensitive it will be to the

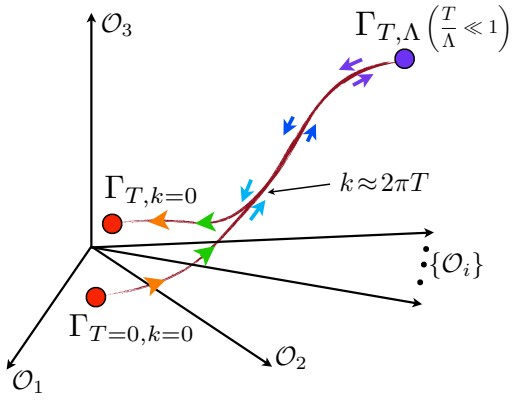

FIG. 6: Flow at vanishing temperature from $k=0$ to $k=\Lambda$, and flow at $T\neq 0$ from $k=\Lambda$ to $k=0$ with $\Lambda/T\gg 1$. The flow is described in theory space, and the axes label (orthogonal) couplings/observables $\mathcal{O}_i$ which serve as expansion coefficients of the effective action, e.g. $\mathcal{O}_1=\Gamma^{(2)}(p=0)$. The flows start to deviate at $k\approx T$, see the discussion below.

approximation at hand. Eventually, the polynomial contributions to the flow integrate up to the standard thermal exponential suppression, that relates to the thermal distribution functions as discussed in Section III.

We conclude that we have a polynomial decay in the flow, which indeed plays a rôle for computing quantitatively reliable thermodynamic quantities. Additionally, we can utilise the ideas about locality to preserve as much as possible of the exponential decay, that stabilises any approximation scheme. We turn to the localised version of the flow derived in the previous Section III. As the flow of $\hat{\Gamma}_k^{(2)}$ vanishes identically for momenta larger than λk for all temperatures T we arrive at

$$\Delta\hat{\Gamma}^{(2)}_{T,\Lambda}(p)=0+O(e^{-\Lambda/T})\,, \tag{39}$$

where we have neglected the backreaction of the polynomial decay of the thermal corrections of higher correlation functions. The two-point function is the most important quantity if it comes to the computation of thermodynamic observables. It is exactly here where the locality-preserving flow pays off in quantitative reliability.

Finally, we are interested in the correlation functions $\Gamma^{(n)}$ at $k=0$, which have to be computed from the $\hat{\Gamma}^{(n)}$ via the rescaling with powers of $\hat{Z}_{k=0}$. At vanishing temperature we have used the natural normalisation $\hat{Z}_{k=0}=1$, see (32) and (33), and the two sets of correlation functions agreed at $k=0$. At finite temperature we initiate the flow at $k=\Lambda$ with T/Λ. Here we have (39) for the difference of the localised correlation functions, and we use the natural definition

$$\hat{Z}_\Lambda(p;T):=\hat{Z}_\Lambda(p;T=0)\,. \tag{40}$$

Eq. (40) implies that (39) also applies to $\Delta\Gamma^{(2)}_{T,\Lambda}$: at the UV scale we have exponentially suppressed thermal fluctuations for the two-point function. As we expect a polynomial suppression due to the arguments in Section III, the use of the computational simple initial condition amounts to a temperature-dependent renormalisation of $\Gamma_k^{(n)}(T)$ at non-vanishing cut-off scale k. For the same reason, (40) also leads to $Z_{k=0}(p;T)\neq 1$, and we have to compute it from the flow of $\hat{\eta}_k$. We have

$$\begin{aligned}\hat{Z}_k(p;T) &= \hat{Z}_\Lambda(p;0)\,\exp\left\{\int_\Lambda^k dt'\,\hat{\eta}_k(p;T)\right\}\\ &= e^{\int_0^k dt'\,\hat{\eta}_k(p;0)}\,e^{\int_\Lambda^k dt'\,(\hat{\eta}_k(p;T)-\hat{\eta}_k(p;0))}\,,\end{aligned} \tag{41}$$

where we have used (32) in the second line of (41). The relation (41) entails that the rescaling factor $Z_{k=0}(p;T)$ contains the thermal part of the momentum transfer.

V. APPROXIMATION

In this section we discuss the approximation scheme used to capture the thermal fluctuations and thus allows for a quantitative computation of the temperature-dependence of the propagators.

In general, the structure of the flow of the effective action, see Figs. 2,3, entails that flows of n-point functions depend explicitly on $(n+2)$-point functions. The relevant example for the present work is the flow of the (inverse) Yang-Mills propagators $\Gamma_k^{(2)}$, displayed in Fig. 4. The flows depends on $\Gamma_k^{(n)}$ with $n\leq 4$. In other words, the functional flow in eq. (5), if broken up in the flows of n-point functions, constitutes an infinite hierarchy of coupled integro-differential equations. For computational purposes the system must be closed: the set of potentially contributing operators must be rendered finite, such that the relevant physics is kept in the approximation. Moreover, the approximation should be subject to self-consistency checks that give access to the systematic error.

First, let us describe the approximation put forward here for the flow of the propagators in Fig. 4, before we put down the explicit parameterisation/approximation in terms of $\Gamma_k^{(n)}$ with $n\leq 4$: we keep the full propagators and work with self-consistent approximations to the vertices which respect the renormalisation group properties of the vertices. We also use the flow equation for the ghost-gluon vertex, evaluated at the symmetric point with $p_i^2=k^2$, $i=1,2,3$, for the momenta of ghost, antighost and gluon, respectively. We have checked the reliability of the RG-consistent ansatz for the three-gluon vertex with its flow at the symmetric point $p^2=k^2$. The reliability of the RG-consistent four-gluon vertex is checked by its DSE computed in [55].

A. Two-point functions and their flows

Now we proceed with the parameterisation of our approximation. We concentrate on the localised two-point functions $\hat{\Gamma}^{(2)}$, that of the cut-off independent fields are then obtained with (22), (32) and (41). At vanishing temperature the propagators are described by one wave-function renormalisation each, $Z_{A,k}(p)$ and $Z_{c,k}(p)$. At non-vanishing temperature we have to take into account chromoelectric and chromomagnetic modes, the respective projection operators P^L and P^T,

$$\begin{aligned} P^T_{\mu\nu}(p_0,\vec{p}) &= (1-\delta_{\mu 0})\,(1-\delta_{\nu 0})\left(\delta_{\mu\nu} - p_\mu p_\nu/\vec{p}^{\,2}\right), \\ P^L_{\mu\nu}(p_0,\vec{p}) &= \Pi^T_{\mu\nu}(p) - P^T_{\mu\nu}(p_0,\vec{p}), \end{aligned} \tag{42}$$

where $\Pi^T_{\mu\nu}$ is the four-dimensional transversal projection operator, see (15). Thus we parameterise the gluon with two wave-function renormalisations $Z_{L/T}$. The ghost has only a scalar structure at vanishing and finite temperature. The parameterisation of the gluons and ghost is given by

$$\begin{aligned} \hat{\Gamma}^{(2)}_{A,L}(p_0,\vec{p}) &= Z_L(p_0,\vec{p})\,p^2\,P^L(p_0,\vec{p}), \\ \hat{\Gamma}^{(2)}_{A,T}(p_0,\vec{p}) &= Z_T(p_0,\vec{p})\,p^2\,P^T(p_0,\vec{p}), \\ \hat{\Gamma}^{(2)}_{c}(p_0,\vec{p}) &= Z_c(p_0,\vec{p})\,p^2, \end{aligned} \tag{43}$$

where the identity in colour space is suppressed and the $Z's$ are functions of p_0 and $\vec{p}$ separately. The parameterisation of $\Gamma^{(2)}$ follows from that of $\hat{\Gamma}^{(2)}$ in (43), and is read off the definition of $\phi(\varphi)$ in (18) and (29),

$$\Gamma^{(2)}_{A,L/T} \simeq \hat{Z}_{L/T}(p)\,Z_{L/T}(p)\,p^2, \quad \Gamma^{(2)}_{c} \simeq \hat{Z}_c(p)\,Z_c(p)\,p^2. \tag{44}$$

The flow equations for the two-point functions have been given diagrammatically in Fig. 4. Their right hand sides depend on the two-point functions, as well as three- and four-point functions. In particular, we have tadpole diagrams which depend on the ghost-ghost and ghost-gluon scattering vertices $\Gamma^{(4)}_{\bar{c}c\bar{c}c}$ and $\Gamma^{(4)}_{\bar{c}A^2c}$, respectively. These vertices vanish classically, and in a first approximation one is tempted to drop the related diagrams.

However, they can be considered in a rather simple way, which we use for the flow of the (inverse) ghost propagator: we insert the DSE-relations for $\Gamma^{(4)}_{\bar{c}c\bar{c}c}$ and $\Gamma^{(4)}_{\bar{c}A^2c}$ in the related diagrams. This provides a DSE-resummation of the vertices in a given approximation to the flow. After some straightforward but tedious algebraic computations, it can be shown that this turns the flow equation for the ghost in Fig. 4 into the total t-derivative of the DSE-equation for the ghost, see Fig. 7. This is nothing but the statement that a flow equation for a correlation function can be seen as the differential form of the corresponding DSE for the ghost two-point function in the presence of the regulator term; both describe the same correlation function. The ghost-DSE and its t-derivative is illustrated in Fig. 7. The derivative acting

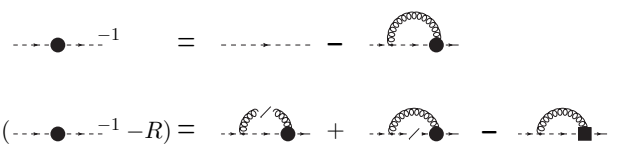

FIG. 7: Flow equation of the ghost propagator from the total t-derivative of the renormalised ghost-DSE. The cutted line stands for the scale derivative acting on the propagator of the corresponding field, see (45). The square denotes the scale derivative acting on the full vertex, the vertex without filled circle denotes the classical vertex.

on the dressed propagator gives

$$\partial_t G[\phi] = -G[\phi]\cdot\partial_t\left(\Gamma^{(2)}[\phi] + R_\phi\right)\cdot G[\phi]\,. \tag{45}$$

The derivative of the bare propagator in the DSE vanishes. The DSE-flow is finite by construction, as it can be derived from the manifestly finite ghost flow in Fig. 4 by inserting the DSEs for the ghost-ghost and ghost-gluon scattering vertices. These DSEs are also manifestly finite and require no renormalisation. To see this explicitly in Fig. 4 we discuss the single terms. First, we note that the total t-derivative of the propagators, $\partial_t G$, shown in (45) act as UV-regularisation of the loops. They decay at least with G^2 as $\partial_t\Gamma^{(2)}_k$ tends towards a constant for large momenta. The total t-derivative $\partial_t\hat{G}$ decays even more rapidly with $\partial_t\hat{R}$ for large momenta due to (30). This reflects again the locality implemented by (30) and its practical importance. The last diagram is proportional to the flow of the ghost-gluon vertex. It will be discussed in detail in the Section V C and is displayed schematically in Fig. 10. Here it suffices to say that the vertex itself is protected from renormalisation and its flow decays rapidly for large momenta.

Both flow equations given in Fig. 4 and Fig. 7 for the ghost are exact and are related via the above resummation procedure. In the present approximation scheme the DSE is more favorable as it only depends on the ghost-gluon vertex, which we shall resolve via its flow. In turn, the four-point functions do not appear explicitly in the total derivative of the DSE, and the related contributions are absorbed in the diagrams with cutted propagators. Notably, the ghost-ghost scattering vertex $\Gamma^{(4)}_{\bar{c}c\bar{c}c}$ disappeared completely from the set of flow equations of ghost and gluon propagators, whereas the ghost-gluon scattering vertex $\Gamma^{(4)}_{\bar{c}A^2c}$ is still present in the flow of the gluon two-point function.

Note that a similar procedure in the flow of the gluon two-point function leads to two-loop diagrams, which are commonly dropped in DSE-computations. This is one of the reasons why we refrain from resumming the related diagrams.

B. Vertices and their flows

For the vertices we first introduce a convenient parameterisation that naturally captures the renormalisation group behaviour. To that end, we utilise the wave function renormalisation of the gluon and the ghost and write

$$\hat{\Gamma}^{(n)}(p_1,...,p_n) = \prod_{i=1}^{n} \bar{Z}_{\phi_i}^{1/2}(p_i)\, \mathcal{T}(p_1,...,p_n)\,. \qquad (46)$$

The $\bar{Z}$-factors are chosen to be proportional to Z, and hence carry the RG-scaling of the vertex as well as the momentum dependence of the legs: they carry potential kinematical singularities, see e.g. [56]. We choose

$$\begin{aligned} \bar{Z}_{L/T}(p) &= \frac{Z_{L/T}(p)\, p^2 - \left[Z_{L/T}(q) q^2\right]_{q=0}}{p^2}\,, \\ \bar{Z}_c(p) &= Z_c(p)\,. \end{aligned} \qquad (47)$$

However, the $\bar{Z}_{L/T}(p)$ are frozen for $p \leq p_{\rm peak}$, where $p_{\rm peak}$ is the potential turning point of the inverse propagator $\Gamma_k^{(2)}$ in the infrared defined by $\partial_p(p^2 Z_{L/T}(p))_{p=p_{\rm peak}} = 0$. The turning point $p_{\rm peak}$ depends on k and tends towards zero for $k \to \infty$. Without this additional constraint $\bar{Z}_{L/T}$ would turn negative for small k, which reflects positivity violation. At finite temperature the turning points depend on T and differ for Z_T and Z_L, the turning point of the latter tends towards *zero* for $T \to \infty$ due to the Debye screening. We emphasise that this is done simply for convenience in order to avoid the splitting of a positive vertex dressing into two negative factors. The $\bar{Z}$'s take into account the RG-scaling of the fields, and reflect the gaps present in the gluonic degrees of freedom.

This leaves us with a renormalisation group invariant tensor $\mathcal{T}$. It is regular up to logarithms and carries the canonical momentum dimension as well as the tensor and colour structure. For the flow of the propagators, Fig. 4, $\mathcal{T}$ has to be computed for the three-gluon and four-gluon vertex, the ghost-gluon vertex, as well as for the four-ghost and ghost-gluon scattering vertices. The latter two, which are absent on the classical level, are treated in terms of exact resummations with the help of DSEs. Now we utilise the locality of the flow: it only carries momenta $q^2 \lesssim k^2$ and is peaked at about $p^2 \approx k^2$. Hence, we approximate the vertices by evaluating them at the symmetric point at $p_i^2 = k^2$ and vanishing temporal components,

$$(p_i)_0^2 = 0 \qquad \text{and} \qquad \vec{p}_i^{\,2} = k^2\,. \qquad (48)$$

Then the $\bar{Z}$-factors in (47) can be evaluated at fixed momenta p with (48) and we set

$$\begin{aligned} \bar{Z}_{k,A} &= \bar{Z}_A(k)\theta(k-k_s) + Z_A(k_s)\theta(k_s-k)\,, \\ \bar{Z}_{k,C} &= Z_C(k)\,, \end{aligned} \qquad (49)$$

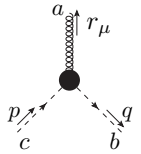

FIG. 8: Ghost-gluon vertex.

where $Z_{k,A}$ is either $Z_{k,L}$ and $Z_{k,T}$, depending on the projection $P^{T/L}$ defined in (42) on the respective leg of $\Gamma_k^{(n)}$. In a slight abuse of notation we have introduced $Z(k)$: the Z-factors in (49) are functions of p_0^2 and $\vec{p}^{\,2}$, which are evaluated at (48). The freezing scale $k_s \propto \Lambda_{\rm QCD}$ in (49) is chosen such that it is bigger than $p_{\rm peak}$. We point out that k_s only defines the parameterisation of the ghost-gluon vertex.

C. Ghost-gluon vertex

It is left to determine the dressings $\mathcal{T}$ for the primitively divergent vertices $\Gamma^{(3)}_{A^3}, \Gamma^{(3)}_{A^4}$ and $\Gamma^{(3)}_{\bar{c}Ac}$, which have a classical counterpart. We restrict ourselves to the classical vertex structure. The evaluation at the symmetric point (48) leaves us with k-dependent dressing functions. For the ghost-gluon vertex we are led to

$$\mathcal{T}^{abc}_{\bar{c}Ac,\mu}(q,p) = z_{k,\bar{c}Ac}\,\frac{1}{g}[S^{(3)}_{\bar{c}Ac}(q,p)]^{abc}_{\mu} = z_{k,\bar{c}Ac}\, iq_\mu f^{abc}\,, \qquad (50)$$

where g is the classical coupling, $S^{(3)}_{\bar{c}Ac}$ is the classical ghost-gluon vertex derived from (2), and p, q are the ghost and anti-ghost momenta respectively, see Fig. 8. The k-dependent factor $z_{k,\bar{c}Ac}$ is RG-invariant and defines a running coupling

$$\bar{\alpha}_s(k) = \frac{z^2_{k,\bar{c}Ac}}{4\pi}\,, \qquad (51)$$

with running momentum scale k. If expanded in powers of the coupling for large momenta, $\bar{\alpha}_s$ has the one and two-loop universal coefficients of the β-function of Yang-Mills theory, where we have used that $\bar{Z}_{k,A} \to Z_{k,A}$ for large cut-off scales.

The flow of $z_{\bar{c}Ac}$ is extracted from that of the ghost-gluon vertex. Here this flow is computed within a DSE-resummation similar to the derivation made for the ghost propagator. Again, the DSE-resummed flow is finite as it is derived from the standard flow equation for the ghost-gluon vertex which is finite by construction. Note however, that already the DSE in Fig. 9 is finite without renormalisation procedure due to the non-renormalisation theorem for the ghost-gluon vertex. Due to simple kinematical reasons, it is also present in approximation schemes that respect the kinematical symmetries.

The above arguments allow us to start straightaway

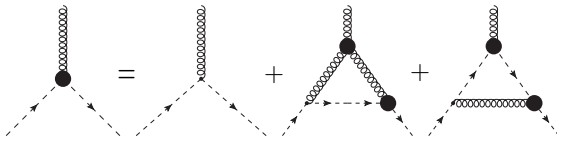

FIG. 9: DSE for the ghost-gluon vertex. The vertex without filled circle denotes the classical vertex.

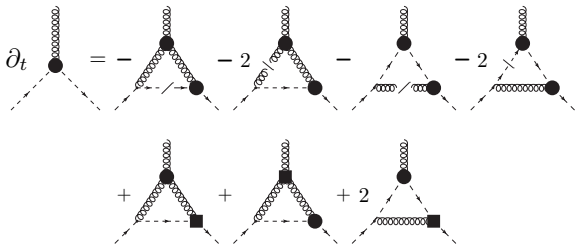

FIG. 10: Flow equation for the ghost-gluon vertex from the total t-derivative of the ghost-gluon vertex DSE in Fig. 9. The cutted line stands for the scale derivative acting on the propagator of the corresponding field, see (45). The square denotes the scale derivative acting on the full vertex, the vertex without a filled circle denotes the classical vertex.

with the simple ghost-gluon DSE, see Fig. 9, which only contains one-loop terms. Similarly to the flow for the ghost propagator, we turn the DSE in Fig. 9 into a flow equation by taking the t-derivative of Fig. 9. The running of the vertex allows for a temperature-dependent computation of the vertex, which will have an important effect in the calculation of the propagators.

It remains to project the vertex flow onto that of the renormalisation group invariant dressing function $z_{k,\bar{c}Ac}$. The projection on the classical vertex structure is done by

$$\Gamma_{\bar{c}Ac}(p_s) = \left(\frac{[\hat{\Gamma}^{(3)}_{\bar{c}Ac}]^{abc}_{\mu} [S^{(3)}_{\bar{c}Ac}]^{abc}_{\mu}}{[S^{(3)}_{\bar{c}Ac}]^{def}_{\nu} [S^{(3)}_{\bar{c}Ac}]^{def}_{\nu}} \right)_{p^2=q^2=(p+q)^2=p_s^2} , \tag{52}$$

with an evaluation at the symmetric point at the momentum scale p_s. For the classical vertex $\Gamma^{(3)}_{\bar{c}Ac} = S^{(3)}_{\bar{c}Ac}$ derived from (2), the dressing is simply unity, $\Gamma_{k,\bar{c}Ac}(p_s) = 1$. In the present approximation we evaluate the vertices at the moment scale k, and hence we define

$$\Gamma_{k,\bar{c}Ac} = \Gamma_{\bar{c}Ac}(k) . \tag{53}$$

Note that the lhs depends on k via the evaluation at $p_s = k$ but also due to the implicit dependence of the vertex on the cut-off scale. The full vertex dressing in (53) also includes the dressing of the legs as split off in (46). Hence, the dressing function $z_{k,\bar{c}Ac}$ is given by

$$z_{k,\bar{c}Ac} = \frac{1}{\bar{Z}^{1/2}_{k,A} \bar{Z}_{k,c}} \Gamma_{k,\bar{c}Ac} . \tag{54}$$

The flow $\partial_t z_{k,\bar{c}Ac}$ is determined from (54) and is directly related to that of the ghost-gluon vertex. Taking the t-derivative of (54) leaves us with

$$\left(\partial_t + \frac{1}{2} \frac{\partial_t \bar{Z}_{k,A}}{\bar{Z}_{k,A}} + \frac{\partial_t \bar{Z}_{k,c}}{\bar{Z}_{k,c}} \right) z_{k,\bar{c}Ac} = \partial_t \Gamma_{k,\bar{c}Ac} \frac{1}{\bar{Z}^{1/2}_{k,A} \bar{Z}_{k,c}} .$$

The scale-derivative of the full dressing $\Gamma_{\bar{c}Ac}$ is proportional to the flow of the vertex but also to the derivative with respect to the momentum at the symmetric point,

$$\partial_t \Gamma_{k,\bar{c}Ac} = \left[\partial_t \Gamma_{\bar{c}Ac}(p_s) + p_s \partial_{p_s} \Gamma_{\bar{c}Ac}(p_s) \right]_{p_s=k} .$$

Upon integration the flow (54) gives us the vertex dressing of the ghost-gluon vertex at a given cut-off scale k,

$$z_{k,\bar{c}Ac} = z_{k=0,\bar{c}Ac} + \int_0^k \frac{dk'}{k'} \partial_{t'} z_{k',\bar{c}Ac} . \tag{55}$$

For the thermal flows in the present work the initial condition $z_{k=0,\bar{c}Ac}|_{T=0}$ is required. It is here where we take advantage of the progress made over the last two decades in our understanding of Landau gauge QCD at vanishing temperature, for a review see [30]. At vanishing temperature a one-parameter family of solutions with infrared enhanced ghost propagators and gapped gluon propagators in Landau gauge has been found. All solutions have a gluon propagator with a mass gap $m_{\rm gluon} \propto \Lambda_{\rm QCD}$. They only differ from each other in the deep infrared for momenta $p^2 \ll \Lambda_{\rm QCD}$. There the gluon propagator is described by

$$Z_A(p \ll \Lambda_{\rm QCD}) \propto c(p) \frac{m^2_{\rm gluon}}{p^2} , \tag{56}$$

where $c(p) \gtrsim 1$ is a momentum-dependent function which is bounded from below. For all solutions but one $c(p)$ it is also bounded from above, these solutions are called decoupling solutions, as the gluon decouples in that momentum regime. There is one distinguished member of this family where $c(p)$ diverges with $p^{2+2\kappa_A}$ with $\kappa_A < -1$, see [30]. This solution is called scaling solution as the infrared propagators and vertices are uniquely determined by scaling laws up to constant prefactors, see e.g. [30, 56–61].

Most importantly, the flow of the ghost-gluon vertex in Fig. 10 is not sensitive to the infrared behaviour of the gluon propagator. All diagrams in Fig. 10 vanish in the limit $k \to 0$ with powers of $k^2/m^2_{\rm gap}$,

$$\lim_{k\to 0} \partial_t z_{k,\bar{c}Ac} \propto \frac{k^2}{m^2_{\rm gap}} . \tag{57}$$

This also entails that the vertex dressing tends toward a constant in the infrared. Hence, we infer that the

infrared value of the ghost-gluon vertex is the same for the whole class of solutions up to subleading terms in RG-transformations. This can be used to compute $z_{k=0,\bar{c}Ac}|_{T=0}$ for the whole class of solutions. It has been shown that the scaling solution for constant ghost-gluon dressings is determined in the FRG up to an RG-constant, see [62],

$$z^2_{k=0,\bar{c}Ac}\big|_{T=0}\left(\frac{\bar{Z}_A(p)\bar{Z}^2_c(p)}{Z_{A,s}(p)Z^2_{c,s}(p)}\right)_{p=0} = 4\pi\alpha_{s,\mathrm{IR}}\,, \quad (58a)$$

with the scaling wave function renormalisations $Z_{A/C,s}$ for ghost and gluon propagators, respectively. The coupling $\alpha_{s,\mathrm{IR}}$ is analytically known, see [58],

$$\alpha_s = -\frac{4\pi}{N_c}\frac{2}{3}\frac{\Gamma(-2\kappa)\Gamma(\kappa-1)\Gamma(\kappa+3)}{\left(\Gamma(-\kappa)\right)^2\Gamma(2\kappa-1)} \overset{N_c=3}{\approx} 2.97\,, \quad (58b)$$

where $\kappa \approx 0.595$.

For momenta $p \gg \Lambda_{\mathrm{QCD}}$ the $Z_{A/C,s}(p)$ tend towards the decoupling solutions up to RG-scalings. Demanding equivalence for large momenta fixes the relative ultraviolet renormalisation condition. In summary, this allows us to fix $z^2_{k=0,\bar{c}Ac}$ at vanishing temperature for a given set of scaling or decoupling propagators in terms of the UV renormalisation condition.

In the light of the ongoing debate about the infrared behaviour of Landau gauge propagators in the vacuum ($T = 0$) it is important to stress the following: first, the flow of the vertex function is not sensitive to the differences of the momentum behaviour of the propagators in the deep infrared, $p \ll \Lambda_{\mathrm{QCD}}$, as it is switched off for $k \to 0$ below Λ_{QCD}. Second, the above argument leading to (58) only relies on the technical possibility of finding initial ultraviolet conditions for the flow in the given approximation which flow into the scaling solution in the infrared. This is trivially possible, see [30, 62, 63]. Then, the analytical values of the scaling solution fixes (58) for both, scaling and decoupling solutions. This does not resolve the infrared problem in Landau gauge Yang-Mills theory closely related to the picture of confinement, as well as to the resolution of the Gribov problem in this gauge.

At non-vanishing temperature the coupling is suppressed below the temperature scale $k \sim T$, see e.g. [28]. Furthermore, we have to distinguish between transversal and longitudinal gluon legs. If all Matsubara frequencies vanish, $p_0 = q_0 = 0$, the longitudinal vertex vanishes and the distinction is only relevant for non-vanishing Matsubara frequencies. There, however, all (hatted) quantities quickly tend towards their $T = 0$ counter parts. Therefore, we approximate the longitudinal vertex dressing at finite temperature by the transversal one,

$$z^L_{k,\bar{c}Ac} = z^T_{k,\bar{c}Ac}\,. \quad (59)$$

In summary, we have set up a relatively simple flow for the ghost-gluon vertex which already covers the quantitative features of the full vertex flow. We have also checked our approximation by computing the full vertex flow on the basis of the results in the present approximations. This also provides us with an estimate of the systematic error in the present approximation. A full analysis of this will be published elsewhere.

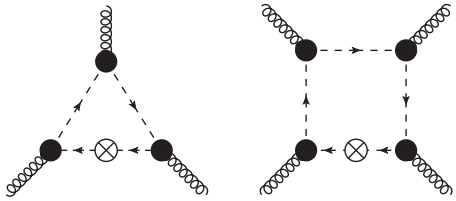

FIG. 11: Infrared dominating diagrams in the flow equations for the three-gluon vertex and the four-gluon vertex.

D. Gluonic vertices

It remains to determine the purely gluonic vertices. They are described within a parameterisation similar to (50). We have schematically

$$\mathcal{T}_{A^3} = z_{k,A^3}\,\frac{1}{g}S^{(3)}_{A^3}\,, \qquad \mathcal{T}_{A^4} = z_{k,A^4}\,\frac{1}{g^2}S^{(4)}_{A^4}\,, \quad (60)$$

where the vertex dressings z_{k,A^3} and z_{k,A^4} relate directly to the ghost-gluon dressing $z^2_{k,\bar{c}Ac} = 4\pi\bar{\alpha}_s(k)$, (51), for large cut-off scales $k \gg \Lambda_{\mathrm{QCD}}$ or large momenta due to two loop universality.

Indeed, this reasoning has been validated in [55] with DSE-equations for the four-point coupling. Hence, we have $z_{k,A^4} \simeq z^2_{k,\bar{c}Ac}$ for most of the momentum regime with a potential deviation in the deep infrared for $k^2/\Lambda^2_{\mathrm{QCD}} \ll 1$. We parameterise accordingly

$$z_{k,A^3} = z_3\, z_{k,\bar{c}Ac}\,, \quad \alpha_{s,A^4} = z_4\, z^2_{k,\bar{c}Ac}\,, \quad (61)$$

where the $z_i, i = 3, 4$, are functions which are expected to approach unity for $k^2 \gtrsim \Lambda^2_{\mathrm{QCD}}$, that is

$$z_{i,k\gg\Lambda_{\mathrm{QCD}}} \to 1\,, \quad (62)$$

for $i = 3, 4$. Their infrared behaviour is determined by the only diagram in the flow that does not depend on the gapped gluon propagator, see Fig. 11. The effect of these diagrams on the vertices is determined by two competing effects:

First, these diagrams are suppressed due to their colour structures and the related vertex dressings are suppressed relative to that of the ghost-gluon vertex. In the case of the four-gluon vertex this combinatorial suppression is of order $10^2 - 10^3$, which is nicely seen in the solution in [55]. For the three-gluon vertex the combinatorial suppression factor also turns out to be of order $10^2 - 10^3$, subject to the chosen momenta, details will be published

elsewhere. This factor has been determined within a two-dimensional lattice study as 0.017, [64].

Second, these diagrams grow strong in comparison to the respective diagram in the flow of the ghost-gluon vertex, which involves one gapped gluonic propagator. In the decoupling case the flow of the gluonic vertices for $k \to 0$ is proportional to k^0 up to logarithms. This leads to an effective suppression of diagrams with gluonic vertices as such diagrams also involve gapped gluon propagators, and hence a suppression with $k^2/m^2_{\rm gap}$. In the scaling case the diagrams with gluonic vertices decouple with powers of the scaling, which can be seen best in the DSE-hierarchy.

In summary, the above analysis entails that we can safely drop the related diagrams for $k \leq \Lambda_{\rm QCD}$, and above this scale the vertices have a dressing similar to that of the ghost-gluon vertex. In the vertices we have factorised the multiplicative dressing functions $\bar{Z}^{1/2}$ for the respective legs that are at our disposal. In turn, the relative thermal suppression factor is safely encoded in the ratio of the full ghost-gluon vertex dressings at vanishing and finite temperature,

$$\frac{\Gamma_{k,\bar{c}Ac}|_T}{\Gamma_{k,\bar{c}Ac}|_{T=0}} \,. \tag{63}$$

Since the temperature dependent dressing factor $z_{\bar{c}Ac}$ has already been included in the definition (61), we deal with the reduced ratio of the wave function renormalisations,

$$r_{\bar{c}Ac}(k,T) = \frac{\bar{Z}^{1/2}_{k,A}\,\bar{Z}_{k,C}\Big|_T}{\bar{Z}^{1/2}_{k,A}\,\bar{Z}_{k,C}\Big|_{T=0}} \,, \tag{64}$$

leading to the final approximation of the gluonic vertex dressings by

$$z_i(k,T) = r_{\bar{c}Ac}(k,T)^{i-2} \,, \quad z_i^{\rm min}(k,T) = \frac{\bar{Z}_{k,A}}{Z_{k,A}} z_i(k,T) \,. \tag{65}$$

The results we show are achieved within the second set of vertex dressings, where we additionally switch-off the gluonic vertices linearly below the temperature scale, which implements the additional thermal suppression in the infrared. This betters the numerical convergence. In Section VII we test the sensitivity of the results to this switch-off.

At non-vanishing temperature the structure functions z_{A^n} also have to carry the difference between the coupling to longitudinal and transversal gluons, which is relevant for the second choice in (65). The ratio $\bar{Z}_A/Z_A$ goes to $\bar{Z}_{L/T}/Z_{L/T}$. The validity of the present approximation is then tested by computing the flow of z_{A^3} on the basis of our results. Note also that $z_{k,\bar{c}Ac}$ only has transversal parts as we evaluate the flows at vanishing Matsubara frequency.

E. Regulators

For a numerical treatment of finite temperature flow equations, exponential regulators

$$r_m(x) = \frac{x^{m-1}}{e^{x^m}-1} \tag{66}$$

generally provide good numerical stability. The parameter m controls the sharpness of the regulator, which directly relates to the locality of the flow. As already pointed out in section III, locality is a central issue. The importance of sufficiently local flows is also seen on the level of the regulator, where it turns out that the non-locality induced by the exponential regulator (66) with $m = 1$ spoils the stability of the flow. On the other hand, regulators with a steep descent lead to a slower convergence of the regularised thermal propagators and vertices towards the vacuum ones at $T = 0$. Indeed, for sharp cut-off functions or non-analytic ones thermal modifications are present for arbitrarily large cut-off scales Λ. This invalidates the use of the $T = 0$ initial conditions at the initial UV scale Λ. Accordingly, we use $m = 2$ in the computation, whose form is shown in Fig. 1. The full regulators for the gluon and the ghost are given by

$$\begin{aligned} \hat{R}^{T/L\,ab}_{\mu\nu}(p) &= \delta^{ab} P^{T/L}_{\mu\nu}\, \bar{Z}_{k,T/L}\, p^2 r_2(p^2/k^2) \,, \\ \hat{R}^{ab}(p) &= \delta^{ab}\, Z_c(0)\, p^2 r_2(p^2/k^2) \,, \end{aligned} \tag{67}$$

with the projection operators $P^{L/T}$ defined in (42). We have chosen $Z_c(0)$ instead of $Z_c(k)$ for numerical convenience. The ghost renormalisation function $Z_c(p;T)$ tends towards zero for small momenta and finite temperatures. It is a balance between ghost propagator, gluon propagator and ghost-gluon vertex, which prohibits Z_c getting negative. This balance is better resolved numerically with the prefactor $Z_c(0)$ in the regulator R_c for the ghost. At vanishing temperature we have $\bar{Z}_{k,L} = \bar{Z}_{k,T}$, and the gluon regulator $R_{k,A} = R^T + R^L$ is proportional to the four-dimensional transversal projection operator Π defined in (42), see also the discussion below (4).

VI. COMPUTATIONAL DETAILS

The discussion of the last section leaves us with a coupled set of partial integro-differential equation depicted in Fig. 12. The initial condition is set in the vacuum, $T = 0$, at vanishing cut-off scale, $k = 0$. The vertices are determined by (58b) and the relations in the Sections V C,V D and the input gluon and ghost propagators are taken from [30], from which we choose a decoupling solution.

In order to solve the flow equation up to a UV scale Λ we adopt an iteration procedure, which is very stable for the direction $k \to \Lambda$. Herein the iteration $(i+1)$ only

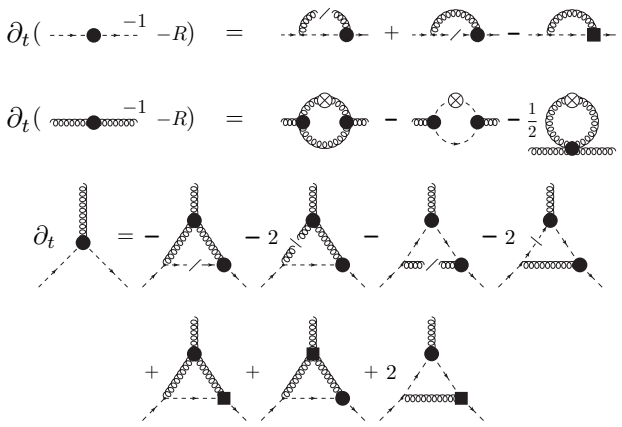

FIG. 12: Yang-Mills flows for propagators and ghost-gluon vertex in the approximation discussed in Section V. The flows for the ghost propagator and the ghost-gluon vertex are DSE-resummed and the ghost-tadpole in the gluon equation is neglected.

depends on the given solution (i),

$$\Gamma^{(n)}_{k,i+1} = \Gamma^{(n)}_{k=0,i} + \\ + \int_0^k \frac{dk'}{k'} \mathrm{Flow}^{(n)}_{i+1}\left(\Gamma^{(n)}_{k,i}, \mathrm{Flow}^{(n)}_{i}\right) . \quad (68)$$

Incrementing the number of iterations until the solution is stable under further iteration, i.e. $\Gamma^{(n)}_{k,m+1} = \Gamma^{(n)}_{k,m}$ up to desired accuracy, gives the solution of the flow equation. The starting point of the iteration we take as $\Gamma^{(n)}_{k,(0)} = \Gamma^{(n)}_{T=0,k=0}$. Then we converge within the iterations rapidly to the initial condition $\Gamma^{(n)}_{\Lambda,T=0}(p^2)$.

In contrast to the direction $k \to \Lambda$ in the zero temperature case, the flow from high to low scales at finite temperature involves instabilities. This is due to the self-regulating nature of the equations for the wave-function renormalisation of the ghost in combination with the ghost-gluon vertex dressing. Their structure is such that if one of the quantities becomes small it stops the flow of the other and in the following also its own flow, which is what happens at finite temperature. However, as soon as one of these quantities happens to be negative in an intermediate iteration step, the iteration becomes unstable, i.e. each iteration step brings the iteration solution further away from the correct solution. The system is highly sensitive to this, as one has to resolve very small values numerically. Therefore, we pursue a more direct strategy to solve the flow, namely an evolution of the flow according to a Runge-Kutta solver

$$\Gamma^{(n)}_{k_{i-1}} = \Gamma^{(n)}_{k_i} + \frac{k_{i-1} - k_i}{k_i} \mathrm{Flow}^{(n)}_{k_i}, \quad (69)$$

from the starting condition $k_N = \Lambda \gg T$ to $k_0 = 0$. In the evolution the system reacts on the balancing effect between the ghost propagator and ghost-gluon vertex immediately, and the purely numerical problem of possibly negative values of Z_c or $z_{\bar{c}Ac}$ in the iteration is avoided. Note that the result is stable under iteration again, as it is the exact solution of the equation. The sensitivity to the balancing is still present, but shows up in the form of a small evolution step size of $|k_{i-1} - k_i| \lesssim 10$MeV.

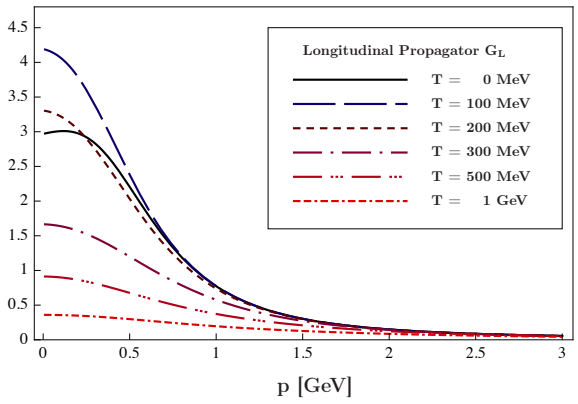

FIG. 13: Longitudinal gluon propagator G_L at different temperatures as a function of spatial momentum.

VII. RESULTS FOR PROPAGATORS AND VERTICES

In this section we present the results for the ghost and gluon propagators and the ghost-gluon vertex. The temperature is given in lattice units. As has been argued in section IV, the results for the ghost and gluon propagators show the typical thermal scale $2\pi T$. Below this scale we have significant temperature effects on the momentum dependence. In turn, above this scale the temperature fluctuations are suppressed and all propagators tend towards their vacuum counterparts at vanishing temperature. This also holds true for the ghost-gluon vertex. This supports the self-consistency and stability of the thermal flows as discussed in section IV.

The most significant effect can be seen for the chromoelectric and chromomagnetic gluon propagators, that is the components of the propagator longitudinal and transversal to the heat bath. The zero mode of the longitudinal gluon propagator at various temperatures is given in Fig. 13 as a function of spatial momentum. For low temperatures $T \lesssim 150$ MeV we see an enhancement of the longitudinal propagator. Such an enhancement is also seen on the lattice, [15, 17, 35, 36, 41, 42]. It has been emphasised on the basis of the FRG that specifically the propagator of the electric mode should show critical behaviour, if computed in the background fields that solve the non-perturbative equations of motion [35]. However, the significance of the lattice results so far as well as quantitative details are not settled yet. For higher temperatures the longitudinal propagator is suppressed

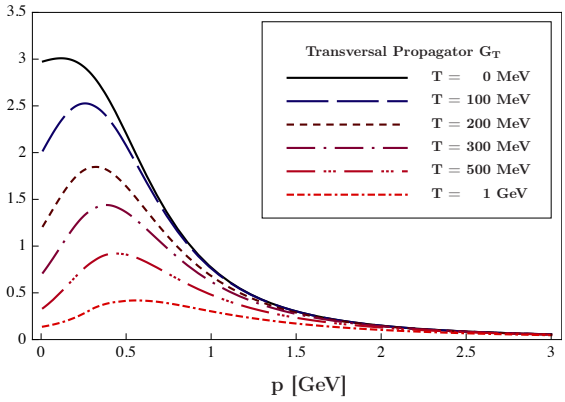

FIG. 14: Transversal gluon propagator G_T at different temperatures as a function of spatial momentum.

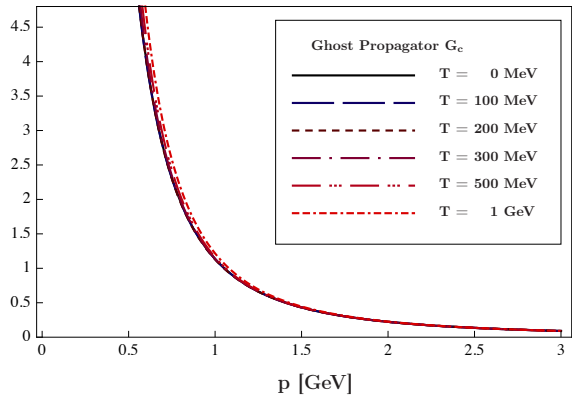

FIG. 15: Ghost propagator G_c at different temperatures as a function of spatial momentum.

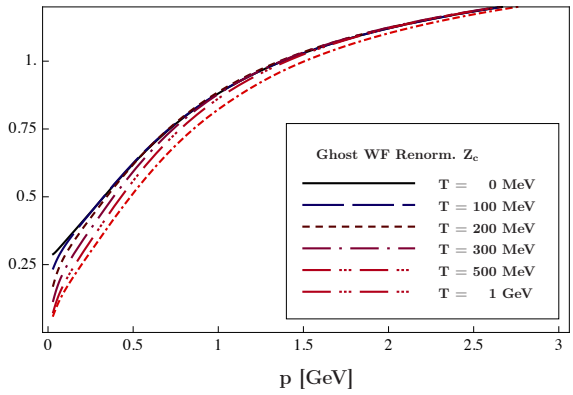

FIG. 16: Zero mode of the wave-function renormalisation of the ghost Z_c at different temperatures as a function of spatial momentum.

relative to the gluon propagator at vanishing temperature. This is the expected behaviour caused by the Debye screening mass due to the thermal screening of the chromoelectric gluon. For asymptotically high temperatures $T \gg T_c$ the chromoelectric gluon decouples. The onset of this behaviour at about $T \approx 200$ MeV is earlier as in the respective lattice computations [15, 17, 35, 36, 41, 42] where the thermal decoupling takes place for temperatures larger than the critical temperature.

In order to capture this behaviour we have to extend our present truncation with a self-consistent inclusion of the Polyakov loop background as well as a better resolution of the purely gluonic vertices for momenta and frequencies below $\Lambda_{\rm QCD}$. Both extensions are under way, and the results will be presented elsewhere. In turn, for large temperature and momentum scales above $\Lambda_{\rm QCD}$ the above lack of quantitative precision at infrared scales is irrelevant. Here we see quantitative agreement with the lattice results, see Fig. 22.

The transversal mode is not enhanced for small temperatures, in clear distinction to the longitudinal mode. It is monotonously decreased with temperature, see Fig. 14. Moreover, it develops a clear peak at about 500 MeV. This can be linked to positivity violation, which has to be present for the transversal mode: in the high temperature limit it describes the remaining dynamical gluons of three-dimensional Yang-Mills theory in the Landau gauge. The infrared bending is more pronounced as that of respective lattice results, and its strength is subject to the lack of quantitative precision at these scales. In turn, for larger momenta the transversal propagator agrees well with the respective lattice propagator. The ghost only shows a small temperature dependence, in contradistinction to the gluonic propagators. This is fully compatible with the lattice results, see [15, 17, 35, 36, 41, 42]. The temperature dependence is hardly evident on the level of the propagator, see Fig. 15, but can be resolved on the level of the wave-function renormalisation, see Fig. 16. The wave-function renormalisation is slightly suppressed, which corresponds to a successive enhancement of the ghost propagator at finite temperature. The enhancement of the ghost propagator is potentially self-amplifying, as it feeds back into the flow of the ghost two-point function, see Fig. 12. This would cause a pole in the ghost propagator at some temperature, if the ghost-gluon vertex did not change. However, in this case the flow of the latter is dominated by the diagrams with two ghost propagators, see Fig. 12, and the ghost-gluon vertex flows to zero.

This non-trivial interplay of the flow of the ghost propagator with the flow of the ghost-gluon vertex leads to a self-stabilising system and prevents a further enhancement of the ghost. This effect is crucial for the stability of the solution of the Yang-Mills system at finite temperature. Indeed, for a constant vertex no solution could be obtained for intermediate temperatures $T \approx T_c$ and above. Thus we conclude that any reliable truncation must comprise direct thermal effects also in n-point functions with $n \leq 3$.

The self-stabilising property of the Yang-Mills system explained above is clearly seen in the temperature-dependence of the ghost-gluon vertex. The vertex is sup-

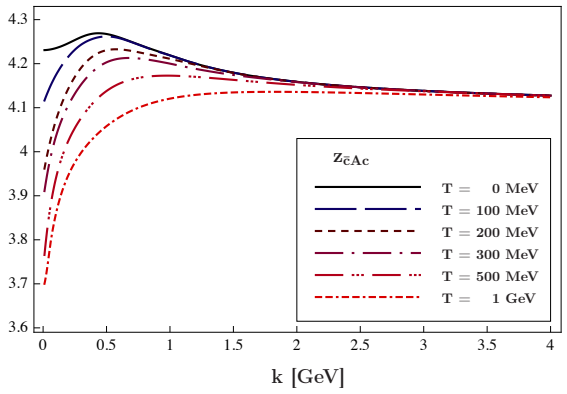

FIG. 17: Dressing function $z_{\bar{c}Ac}$ of the ghost-gluon vertex at different temperatures as a function of spatial momentum.

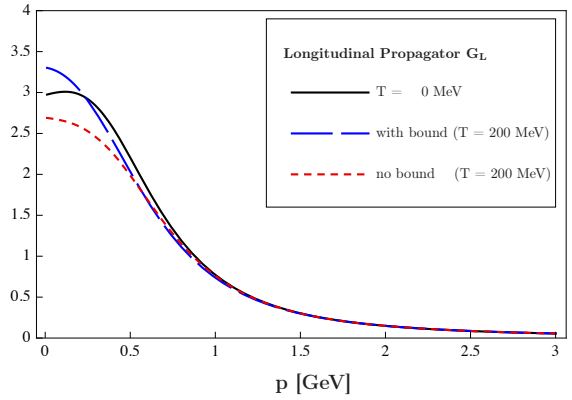

FIG. 18: Comparison of longitudinal propagator with minimal and maximal strength of the coupling of purely gluonic vertices.

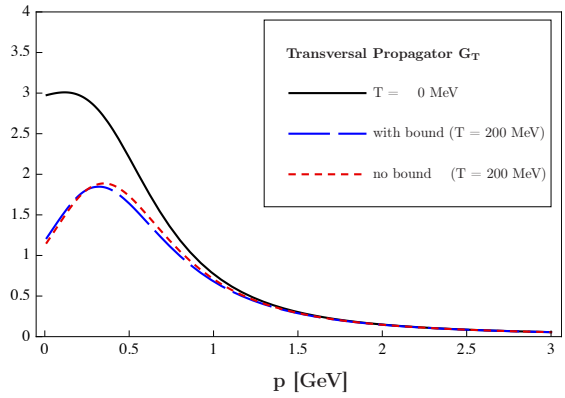

FIG. 19: Comparison of transversal propagator with minimal and maximal strength of the coupling of purely gluonic vertices.

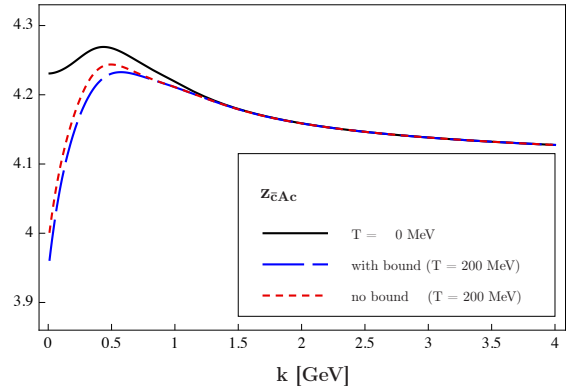

FIG. 20: Comparison of ghost-gluon vertex with unbounded and bounded gluonic flow.

pressed successively with the temperature, see Fig. 17, which in turn ensures the relatively mild change of the ghost propagator. Especially the sharp drop-off of the vertex at small scales k accounts for the smallness of the thermal fluctuations to the ghost propagator.

In Section V D, we approximated the temperature dependence of the gluonic vertices by an ansatz that combined all necessary qualitative properties of the vertices. In order to check the sensitivity of the propagators at low temperatures to this choice, we compare the results with a strong suppression with a computation where the minimal suppression of the gluonic vertices defined in eq. (65) is implemented. This gives an approximate error band for the propagators with respect to the ansatz of the gluonic vertices. We find that the main impact of the truncation of the gluonic vertices is onto the longitudinal propagator below T_c, given in Fig. 18. We have already mentioned that our truncation has to be improved in order to quantitatively capture the deep infrared, and the temperature dependence of the gluonic vertices is an important ingredient.

In contrast to the sensitivity of the deep infrared behaviour of the longitudinal gluon, the transverse gluon propagator, see Fig. 19, as well as the ghost propagator hardly feel the modified infrared behaviour of the gluonic n-point functions. This is in agreement with the well-known fact that the infrared sector of Yang-Mills theory in Landau gauge has ghost dominance (for both scaling and decoupling solutions) for any dimension $d = 2, 3, 4$.

As the wave-function renormalisation of the ghost with the minimal and maximal cut off of gluonic vertices can not be distinguished by eye, we desist from illustrating it explicitly. In contrast to this, the ghost-gluon vertex reflects the switching off of gluonic vertices, see Fig. 20, however, only in a region where the gluonic contributions to the flow are subleading.

In summary, the scheme-dependence of the gluonic vertices affects the details of the thermal decoupling of the longitudinal propagator, but has no effects on the transversal propagator and the ghost. The sensitivity of the thermal decoupling of the propagator to the thermal decoupling of the vertices is easily understood. In turn, transversal gluon and ghost are the relevant de-

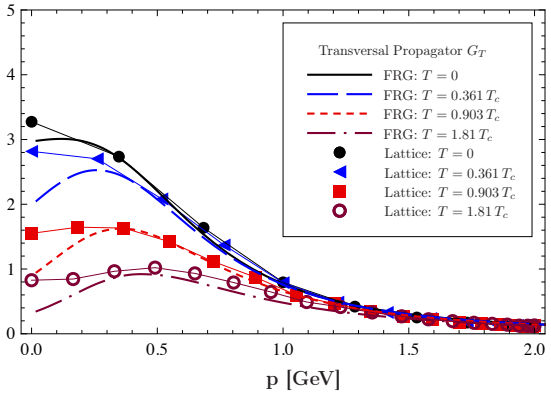

FIG. 21: Transversal gluon propagator in comparison with lattice results [35, 42]. The lattice data has been rescaled such that the $T = 0$ propagators match at intermediate momenta $p \gtrsim 1$ GeV.

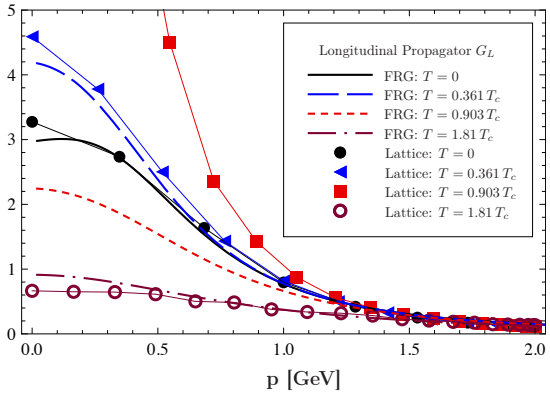

FIG. 22: Longitudinal gluon propagator in comparison with lattice results [67]. The lattice data has been rescaled such that the $T = 0$ propagators match at intermediate momenta $p \gtrsim 1$ GeV.

grees of freedom for asymptotically high temperatures where we are led to a three-dimensional confining theory. This property can be seen nicely on the lattice, where only the transversal gluon is sensitive to the removal of confining configurations, see e.g. [65]. We conclude that our approximations do not affect the confining physics.

In the following, we compare the propagators above with lattice results [35, 42, 66]. For this purpose, we scale the lattice data such that the lattice propagators at vanishing temperature match our normalisation at momenta $p \gtrsim 1$ GeV. Take notice that we did not use the lattice propagator as the initial condition, thus the deep infrared of the data deviates from our propagator already at zero temperature, which persists also in the propagators at finite temperature. Apart from that, there is quantitative agreement with the lattice data with respect to the (temperature dependent) momentum region, where the thermal effects appear. In Fig. 21 the transversal propagators are compared. The critical temperature in the lattice data is $T_c = 277\,\text{MeV}$. Clearly, we match the lattice propagator, except for the strong bending of the FRG propagator in the infrared region. This difference is a direct consequence of the mismatch of the ghost and gluon propagators in the deep infrared at vanishing temperature, and relates to the different decoupling solution chosen here. Apart from the deep infrared, the momentum and temperature behaviour of the magnetic gluon matches that of the lattice propagator. In contrast to this, the electric gluon on the lattice shows a qualitatively different behaviour for temperatures below and around the phase transition. Although the longitudinal propagators agree for $T = 0.361 T_c \approx 100\text{MeV}$, it is exactly this region where the uncertainty due to the truncation for the gluonic vertices is large, as shown in Fig. 18 for $T = 200$ MeV. Being aware of a potential truncation dependency in the deep infrared of the longitudinal propagator at low temperatures, we note that in the present truncation the electric gluon shows the onset of the enhancement found on the lattice. Increasing the temperature this feature disappears, and we see a qualitatively different effect for temperatures below T_c. While the continuum result shows a strictly monotonic decreasing propagator, the counterpart on the lattice is enhanced in the confining regime, but reflects the phase transition in form of a rapid decrease at T_c. Nevertheless, this deflection is expected to be missed in the present truncation, as the Polyakov loop potential $V(A_0)$ is pivotal for the critical behaviour around the phase transition. In a full calculation the inverse propagator is proportional to the second derivative of the Polyakov loop $\Gamma^{(2)}_{A,L} \sim V''(A_0)$, see [1, 68–70]. This dependence introduces an additional screening of the vertex-approximations as well as vertex corrections, but in the computations presented here it was dropped. This upgrade should also give us access to the question of the signatures of criticality in the chromoelectric propagator discussed in [15]. Interestingly, such a term is absent in the magnetic modes, which do not depend strongly on the vertex-approximation. It is suggestive that the inclusion of A_0 will further stabilise our computation. However, we defer this interesting computation of the propagator in the presence of a non-trivial background to future work.

VIII. SUMMARY AND OUTLOOK

In the present work we have put forward a functional approach for the quantitative computation of full, momentum dependent correlation functions at finite temperature in Yang-Mills theory. This is done within a FRG-setting which only incorporates thermal fluctuations.

We have computed temperature dependent Yang-Mills propagators and vertices in the Landau gauge for temperatures $T \lesssim 3T_c$. The chromoelectric propagator shows the expected Debye-screening for $T > T_c$ in quantitative

agreement with the lattice results. For small temperatures it shows qualitatively the enhancement also seen on the lattice [15, 17, 35, 36, 38, 41, 42]. However, the significance of the lattice results so far as well as quantitative details are not settled yet. The chromomagnetic propagator shows the expected thermal scaling and tends towards the three-dimensional gluon propagator in quantitative agreement with the lattice. The ghost propagator only shows a mild enhancement with temperature in agreement with the lattice. In contradistinction we see a strong thermal infrared suppression of the ghost-gluon vertex which increases with temperature. The results of this paper are also summarised in [32].

At present we improve on the approximations made here and compute thermodynamic observables such as the pressure and the scale anomaly. The inclusion of the A_0-corrections discussed in Section VII should give access to the properties of the chromoelectric propagator at criticality, see [35]. Furthermore, we utilise the propagators obtained here in a combined approach with FRG and DSE as well as lattice results in an extension of [71]. This work aims at the QCD phase structure for heavy quarks, for lattice results see [6, 72]. Moreover, the glue and ghost propagators are a key input for quantitative computations in full QCD with 2 and 2+1 flavours at finite temperature and density in an extension of [69].

Acknowledgements
We thank R. Alkofer, J.-P. Blaizot, J. Braun, S. Diehl, C. F. Fischer, K. Fukushima, L. M. Haas, M. Ilgenfritz, A. Maas, U. Reinosa, B.-J. Schaefer, A. Sternbeck, L. von Smekal and C. Wetterich for discussions, M. Ilgenfritz, A. Maas, A. Sternbeck for providing lattice results. This work is supported by the Helmholtz Alliance HA216/EMMI. LF acknowledges financial support by the Helmholtz International Center for FAIR within the LOEWE program of the State of Hesse and the Helmholtz Young Investigator Grant VH-NG-322.

[1] J. M. Pawlowski, AIP Conf.Proc. **1343**, 75 (2011), 1012.5075.
[2] D. Binosi and J. Papavassiliou, Phys. Rept. **479**, 1 (2009), 0909.2536.
[3] C. S. Fischer, J.Phys.G **G32**, R253 (2006), hep-ph/0605173.
[4] R. Alkofer and L. von Smekal, Phys. Rept. **353**, 281 (2001), hep-ph/0007355.
[5] C. D. Roberts and S. M. Schmidt, Prog. Part. Nucl. Phys. **45**, S1 (2000), nucl-th/0005064.
[6] O. Philipsen, (2011), 1111.5370.
[7] S. Borsanyi *et al.*, JHEP **1011**, 077 (2010), 1007.2580.
[8] HotQCD collaboration, A. Bazavov and P. Petreczky, J.Phys.Conf.Ser. **230**, 012014 (2010), 1005.1131.
[9] K. Fukushima and T. Hatsuda, Rept.Prog.Phys. **74**, 014001 (2011), 1005.4814.
[10] B.-J. Schaefer, J. M. Pawlowski, and J. Wambach, Phys.Rev. **D76**, 074023 (2007), 0704.3234.
[11] E. Megias, E. Ruiz Arriola, and L. Salcedo, Phys.Rev. **D74**, 065005 (2006), hep-ph/0412308.
[12] C. Ratti, M. A. Thaler, and W. Weise, Phys.Rev. **D73**, 014019 (2006), hep-ph/0506234.
[13] K. Fukushima, Phys.Lett. **B591**, 277 (2004), hep-ph/0310121.
[14] A. Dumitru, Y. Hatta, J. Lenaghan, K. Orginos, and R. D. Pisarski, Phys.Rev. **D70**, 034511 (2004), hep-th/0311223.
[15] A. Maas, (2011), 1106.3942.
[16] B. Grüter, R. Alkofer, A. Maas, and J. Wambach, Eur. Phys. J. **C42**, 109 (2005), hep-ph/0408282.
[17] A. Cucchieri, A. Maas, and T. Mendes, Phys. Rev. **D75**, 076003 (2007), hep-lat/0702022.
[18] J. O. Andersen, L. E. Leganger, M. Strickland, and N. Su, JHEP **1108**, 053 (2011), 1103.2528.
[19] D. F. Litim and J. M. Pawlowski, World Sci. , 168 (1999), hep-th/9901063.
[20] J. Berges, N. Tetradis, and C. Wetterich, Phys.Rept. **363**, 223 (2002), hep-ph/0005122.
[21] J. M. Pawlowski, Annals Phys. **322**, 2831 (2007), hep-th/0512261.
[22] H. Gies, (2006), hep-ph/0611146.
[23] B.-J. Schaefer and J. Wambach, Phys.Part.Nucl. **39**, 1025 (2008), hep-ph/0611191.
[24] J. Braun, (2011), 1108.4449.
[25] O. J. Rosten, (2010), 1003.1366.
[26] M. D'Attanasio and M. Pietroni, Nucl.Phys. **B498**, 443 (1997), hep-th/9611038.
[27] D. Comelli and M. Pietroni, Phys.Lett. **B417**, 337 (1998), hep-ph/9708489.
[28] J. Braun and H. Gies, Phys. Lett. **B645**, 53 (2007), hep-ph/0512085.
[29] D. F. Litim and J. M. Pawlowski, JHEP **0611**, 026 (2006), hep-th/0609122.
[30] C. S. Fischer, A. Maas, and J. M. Pawlowski, Annals Phys. **324**, 2408 (2009), 0810.1987.
[31] L. von Smekal, (2008), 0812.0654.
[32] L. Fister and J. M. Pawlowski, in preparation (2011).
[33] S. Diehl, S. Floerchinger, H. Gies, J. Pawlowski, and C. Wetterich, Annalen Phys. **522**, 615 (2010), 0907.2193.
[34] M. M. Scherer, S. Floerchinger, and H. Gies, (2010), 1010.2890.
[35] A. Maas, J. M. Pawlowski, L. von Smekal, and D. Spielmann, (2011), 1110.6340.
[36] R. Aouane *et al.*, (2011), 1108.1735.
[37] V. G. Bornyakov and V. K. Mitrjushkin, (2010), 1011.4790.
[38] V. Bornyakov and V. Mitrjushkin, (2011), 1103.0442.
[39] A. Cucchieri, F. Karsch, and P. Petreczky, Phys. Lett. **B497**, 80 (2001), hep-lat/0004027.
[40] A. Cucchieri, F. Karsch, and P. Petreczky, Phys. Rev. **D64**, 036001 (2001), hep-lat/0103009.
[41] A. Cucchieri and T. Mendes, (2011), 1105.0176.
[42] C. S. Fischer, A. Maas, and J. A. Müller, Eur. Phys. J. **C68**, 165 (2010), 1003.1960.
[43] U. M. Heller, F. Karsch, and J. Rank, Phys. Lett. **B355**, 511 (1995), hep-lat/9505016.
[44] U. M. Heller, F. Karsch, and J. Rank, Phys. Rev. **D57**, 1438 (1998), hep-lat/9710033.

[45] U. Ellwanger, Phys. Lett. **B335**, 364 (1994), hep-th/9402077.
[46] F. Freire, D. Litim, and J. Pawlowski, Int.J.Mod.Phys. **A16**, 2035 (2001), hep-th/0101108.
[47] S. Tan, Annals Phys. **323**, 2952 (2008), cond-mat/0505200.
[48] S. Tan, Annals Phys. **323**, 2971 (2008), cond-mat/0508320.
[49] S. Tan, Annals Phys. **323**, 2987 (2008), 0803.0841.
[50] J.-P. Blaizot, A. Ipp, R. Mendez-Galain, and N. Wschebor, Nucl.Phys. **A784**, 376 (2007), hep-ph/0610004.
[51] J. Braun, Phys.Rev. **D81**, 016008 (2010), 0908.1543.
[52] D. F. Litim, (1998), hep-ph/9811272.
[53] J.-P. Blaizot, PoS **QCD-TNT09**, 053 (2009), 0912.3896.
[54] J.-P. Blaizot, A. Ipp, and N. Wschebor, Nucl.Phys. **A849**, 165 (2011), 1007.0991.
[55] C. Kellermann and C. S. Fischer, Phys. Rev. **D78**, 025015 (2008), 0801.2697.
[56] C. S. Fischer and J. M. Pawlowski, Phys. Rev. **D80**, 025023 (2009), 0903.2193.
[57] D. Zwanziger, Phys. Rev. **D65**, 094039 (2002), hep-th/0109224.
[58] C. Lerche and L. von Smekal, Phys. Rev. **D65**, 125006 (2002), hep-ph/0202194.
[59] R. Alkofer, C. S. Fischer, and F. J. Llanes-Estrada, Phys. Lett. **B611**, 279 (2005), hep-th/0412330.
[60] C. S. Fischer and J. M. Pawlowski, Phys. Rev. **D75**, 025012 (2007), hep-th/0609009.
[61] R. Alkofer, M. Q. Huber, and K. Schwenzer, Phys. Rev. **D81**, 105010 (2010), 0801.2762.
[62] J. M. Pawlowski, D. F. Litim, S. Nedelko, and L. von Smekal, Phys. Rev. Lett. **93**, 152002 (2004), hep-th/0312324.
[63] C. S. Fischer and H. Gies, JHEP **10**, 048 (2004), hep-ph/0408089.
[64] A. Maas, Phys. Rev. **D75**, 116004 (2007), 0704.0722.
[65] M. N. Chernodub, Y. Nakagawa, A. Nakamura, T. Saito, and V. I. Zakharov, (2011), 1105.4937.
[66] A. Maas, private communication (2011).
[67] C. S. Fischer and J. A. Mueller, Phys. Rev. **D80**, 074029 (2009), 0908.0007.
[68] J. Braun, A. Eichhorn, H. Gies, and J. M. Pawlowski, Eur.Phys.J. **C70**, 689 (2010), 1007.2619.
[69] J. Braun, L. M. Haas, F. Marhauser, and J. M. Pawlowski, Phys. Rev. Lett. **106**, 022002 (2011), 0908.0008.
[70] J. Braun, H. Gies, and J. M. Pawlowski, Phys. Lett. **B684**, 262 (2010), 0708.2413.
[71] C. S. Fischer, Phys. Rev. Lett. **103**, 052003 (2009), 0904.2700.
[72] M. Fromm, J. Langelage, S. Lottini, and O. Philipsen, (2011), 1111.4953.